Development of a supersonic $O(^3P_J)$, $O(^1D_2)$ atomic oxygen nozzle beam source

Steven J. Sibener,[a] Richard J. Buss, Cheuk Yiu Ng,[b] and Yuan T. Lee

Materials and Molecular Research Division, Lawrence Berkeley Laboratory and Department of Chemistry, University of California, Berkeley, California 94720

(Received 11 September 1979; accepted for publication 31 October 1979)

A high pressure, radio frequency discharge nozzle beam source has been developed for the production of very intense ($\geq 10^{18}$ atoms sr^{-1} s^{-1}) supersonic beams of oxygen atoms. An efficient impedance matching scheme has been devised for coupling the radio frequency power to oxygen–rare gas mixtures as a function of gas pressure, temperature, and composition. Techniques for localizing the discharge directly behind the orifice of a specially designed quartz nozzle have also been developed. The above combine to yield a beam source which reliably produces a high degree of molecular dissociation in oxygen–rare gas mixtures at pressures up to 350 Torr. Atomic oxygen mean translational energies from 0.14–0.50 eV have been achieved using the seeded beams technique with Mach numbers up to 10 being realized. When helium is used as the carrier gas both $O(^3P_J)$ and $O(^1D_2)$ atoms are present in the beam, while only ground state atoms appear to be present in argon seeded mixtures. This paper describes the design, construction, and operation of this beam source and provides a characterization of the atomic oxygen beams it has reproducibly generated in our laboratory.

INTRODUCTION

The interactions and reactions of oxygen atoms are of considerable interest and importance due to the fundamental role they play in combustion processes and atmospheric chemistry. The reactions of ground state $O(^3P_J)$ atoms are of particular interest to researchers studying high temperature combustion processes,[1] laser systems based on the reactions of oxygen atoms which lead to products having vibrationally inverted population distributions,[2] and surface chemistry.[3] A thorough understanding of ground state oxygen atom chemistry is also of immediate practical importance since the space shuttle will orbit the earth at altitudes where the major constituent of the atmosphere is $O(^3P_J)$ atomic oxygen. The reactions of excited state $O(^1D_2)$ atoms are of primary importance due to their major role in the chemistry of the stratosphere.[4] The ability of singlet oxygen atoms to insert in a variety of chemical bonds also makes their chemistry a fascinating subject to explore.[5]

In our laboratory a high pressure, supersonic, radio frequency discharge nozzle beam source has been developed in order to determine the products, energetics, and reaction dynamics of atomic oxygen reactions in crossed molecular beam scattering experiments. The motivation for constructing this nozzle beam source, rather than relying on much more simple effusive sources, is that supersonic nozzle sources characteristically produce beams of far greater intensity and smaller translational velocity dispersion than effusive sources.[6] The translational energy of nozzle beams can also be varied over a very wide range, from hypothermal to hyperthermal, by using the seeded beam technique.[7] In this technique the peak velocity of the "seed" gas velocity distribution can ideally approach that of the pure "carrier" gas for very dilute gas mixtures. This is accomplished by accelerating or decelerating the seed gas during hydrodynamic expansion through the nozzle by diluting it in either a lighter or heavier carrier gas. Supersonic beams therefore offer several clear advantages over simple effusive sources for conducting dynamical studies in molecular beam experiments.

The successful operation of a discharge beam source depends strongly on the characteristics of its plasma. In particular, the production of a stable and efficiently coupled high pressure discharge for the generation of atomic species is much more difficult than the production of a low pressure (~1 Torr) discharge. Impedance matching of the plasma to the radio frequency power source as a function of gas pressure, temperature, and composition is required. Plasma localization directly behind the orifice must also be achieved in order to limit atomic recombination before the expansion. Sufficient cooling of the nozzle in order to prevent melting of its orifice, and to limit atomic recombination at the nozzle walls (while not interfering with power coupling to the plasma) is mandatory. Finally, the high pressure plasma must operate in a stable, reproducible, and uniform discharge mode (no beads or streamers) whose temperature is sufficiently high to generate atomic species, but not high enough to melt the orifice of the nozzle. The beam source described in this paper meets all of the above criteria. A boron nitride skimmer is used and is found to be completely stable with respect to the seeded atomic oxygen beam.

Other high pressure atomic oxygen beam sources have been previously reported in the literature. Miller and Patch[8] have described in detail a radio frequency discharge beam source which produces ~35% dissociation at 60 Torr for a 5% oxygen–helium mixture. Gorry

 0034-6748/80/020167-16$00.60

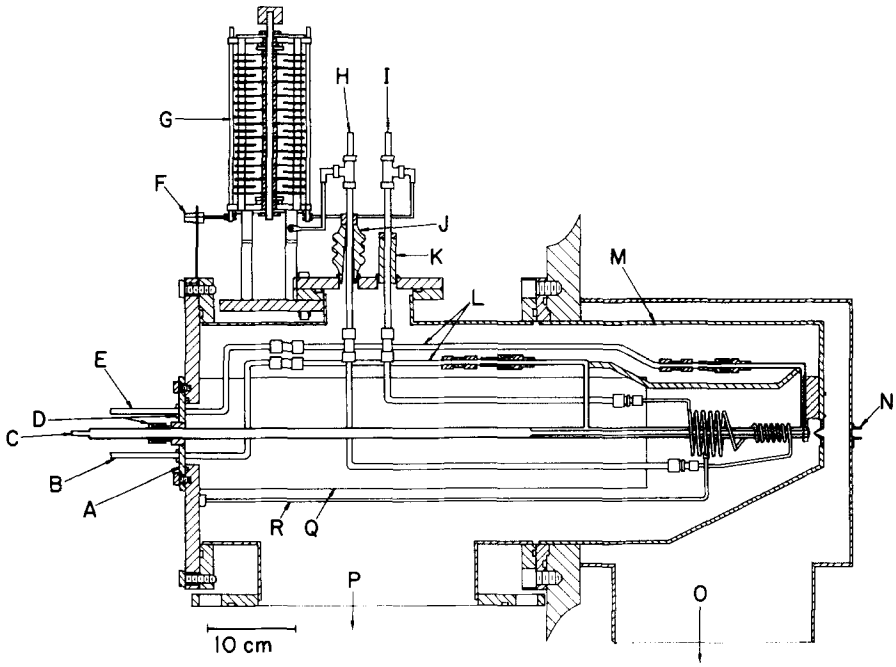

FIG. 1. Sectioned view of the plasma beam source mounted in a differentially pumped chamber. A—lucite insulating flange; B—nozzle coolant return; C—quartz nozzle gas inlet; D—Cajon ultra-Torr fittings; E—nozzle coolant inlet; F—rf power input from RG-213/U coaxial cable; G—variable air capacitor; H—coupling coil coolant outlet; I—coupling coil coolant inlet. J—ceramic feedthrough for rf return and coil coolant; K—ceramic feedthrough for rf input and coil coolant; L—Poly-Flo tubing sections; M—stainless-steel source chamber; N—plates for 5000-V/cm ion deflecting field; O—1200-l/s diffusion pump, differential region; P—4200 or 8000-l/s diffusion pump, source region; Q—epoxy resin mechanical support; R—electrical ground wire. Not shown: wire mesh rf shielding which covers the air capacitor/rf feedthrough assembly.

et al.[9] have reported a microwave discharge source with dissociation characteristics similar to those of Miller and Patch. The impedance matching scheme, nozzle construction and, in particular, plasma localization techniques described in this paper permit a higher degree of molecular dissociation to be achieved at significantly higher operating pressures than the sources mentioned above. The current limitation on the atomic oxygen beam intensity produced by our source is not atomic recombination at high pressures, but rather the speed of the diffusion pump which backs the source region. In some cases the characteristics (for example, gas temperature) of the high pressure plasmas we have generated to date also become a concern when pressures exceeding ~400 Torr are used. The source has been operated at pressures exceeding 200 Torr for oxygen–helium mixtures with greater than 50% molecular dissociation, producing atomic oxygen intensities of $\geq 5 \times 10^{18}$ atoms sr^{-1} s^{-1}. Oxygen–argon mixtures have been discharged at pressures exceeding 300 Torr with greater than 80% dissociation, and with measured atomic oxygen intensities of ca. 5×10^{17} atoms sr^{-1} s^{-1}.

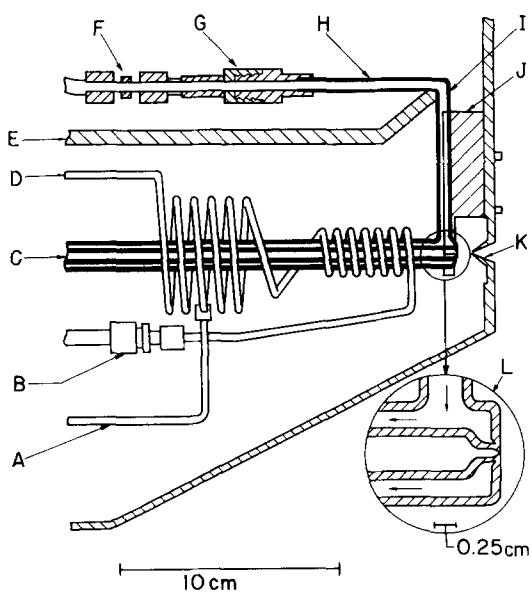

FIG. 2. Sectioned view of the internal source components. A—variable ground tap; B—Swagelock reducer; C—water-cooled quartz nozzle; D—coupling coil; E—quartz support rod for water inlet/outlet assembly; F—Swagelock union joining copper and Poly-Flo tubing; G—Cajon VCO fitting. H—Kovarpyrex section; I—graded seal, pyrex to vycor. J—aluminum support block to electrical ground; K—boron nitride skimmer, 0.88 mm; L—4× enlargement of nozzle tip; arrows indicate low conductivity water flow direction.

The beam source described in this paper was originally designed in order to produce intense supersonic beams of ground state $O(^3P_J)$ atoms. However, we find that when dilute oxygen–helium mixtures are discharged the beam is composed of a mixture of atomic quantum states including excited state $O(^1D_2)$ atoms. The concentration of $O(^1D_2)$ atoms in this beam has proven to be of sufficient magnitude to permit the study of $O(^1D_2)$ reactions in crossed molecular beam experiments. This exciting development will eliminate the need to use powerful and expensive UV pulsed lasers for the photodissociative production of $O(^1D_2)$ atomic beams when the presence of other chemical species in the beam, such as $O(^3P_J)$ and $O_2(^1\Delta g)$, will not seriously complicate the chemistry under study.

I. SOURCE DESIGN AND CONSTRUCTION

A cross-sectional view of the source mounted in the differential pumping region of our universal scattering machine is shown in Fig. 1, with an enlarged view of the internal source components and nozzle tip appearing in Fig. 2. The important design and construction considerations which led to this final form of our plasma beam source will now be discussed.

A. Nozzle construction

The first question to be dealt with was that of nozzle material. Quartz and alumina were the two materials considered based upon their relatively high melting points. Initially 99.8% purity alumina tubes[10] with laser drilled holes were tested. They were unsatisfactory for two reasons. They tended to crack when subjected to large thermal gradients, and arcing occurred between the outer surface of the alumina tubes and the radio frequency coupling coil whenever the outer diameter of the tube came into physical contact with the coil. After this brief test period it was decided that quartz nozzles would have to be fabricated. The final shape of these nozzles can be seen in Fig. 1, C and Fig. 2, C. A water cooling jacket was incorporated in our final nozzle design to prevent the quartz orifice from melting and enlarging during the expansion of the extremely hot gas mixture. The nozzle tip geometry shown in Fig. 2(L) was ultimately found to be stable with respect to orifice enlargement. Here the water coolant flows directly over the junction between the inner, plasma containing tube (6-mm-o.d. commercial grade fused quartz, 1 mm wall thickness, as bubble-free as possible) and the quartz water jacket (12 mm o.d., 1 mm thick). The short tip on the front of the inner tube is approximately 1 mm long and allows the coolant to flow as close as possible to the orifice. This is important due to the poor thermal conductivity of quartz. In addition to preventing melting of the nozzle, water cooling is also desirable since the efficiency of quartz to promote atomic oxygen recombination decreases with lower surface temperatures.[11]

Low electrical conductivity water of 5 μmho/cm conductivity is used as the nozzle coolant and is flowed through the concentric water jacket at a rate of 10 cm^3/s. Use of regular conductivity water as the coolant is precluded due to excessive radio frequency power loss to the water. As an added benefit, the cooling jacket completely eliminated the arcing problem mentioned above. This arcing was found to occur for both alumina and quartz plasma containing tubes which were not physically separated from the coil by another insulating layer.

The nozzle fabrication procedure is quite reproducible and is briefly outlined here. The graded seal water inlet and outlet arms along with their solid quartz support rod (Fig. 2, E, G, H, I) are initially assembled and put aside for later use. Next, the inner tube is prepared. This preparation consists of three operations: Flaring one end just to clear the i.d. of the outer tube, creating the important tip on its front end (Fig. 2, L), and fusing three small quartz physical support standoffs to the inner tube. These three small "droplets" of quartz should be placed at 120° with respect to each other and positioned from 6–7.5 cm from the tip. They should be sized just to clear the i.d. of the outer tube and will be used to hold the inner tube concentric with the water jacket. The inner tube assembly is then slid inside of the outer tube with the outer tube extending past the inner front tip by about 5 cm. At this time the three inner tube support standoffs are fused to the i.d. of the outer tube and should be adjusted until the two tubes are concentric. A ring seal is then made between the flared rear end of the inner tube and the outer tube. Quartz tabulations are then blown onto the outer tube which will ultimately be attached to the water coolant arms. Next, the 5-cm outer tube extension is pared off with a torch and a carbon tool. The objective of this is to create a 1-mm-thick quartz face which seals off the front of the outer tube without touching the tip of the inner tube. This front surface should be as perpendicular as possible to the concentric tube axis and should be just shy of touching the inner tip. The assembly is completed by joining the inner tip and the newly created quartz nozzle face with a ring seal.

At this point the most critical stage of the nozzle fabrication procedure is carried out. The nozzle assembly, with the water arms still detached, is mounted in a glassblower's lathe. The orifice is now blown on a spinning lathe in an operation requiring two people. Using a hydrogen–oxygen flame the front face of the nozzle is heated at a wide angle until the quartz is ready to be blown. The flame is then quickly removed and a hole is blown in the tube. This hole should be slightly larger than the desired diameter of the nozzle orifice. One person now locally heats the tip of the quartz nozzle while the other simultaneously views the hole diameter with a 60× power measuring microscope. The hole is allowed to shrink slowly until the desired diameter is reached. Hole size readjustment can be carried out with this procedure until the orifice is within 0.005 mm of the desired diameter.

When an orifice of the desired size is obtained its straightness is always checked by placing a small positive pressure of oxygen behind the nozzle. This produces a small oxygen jet at the orifice. The shape profile of this jet is then made visible by aiming a small gas torch at the jet while the entire nozzle is rotated in the lathe. If any wobble or precession of the flame jet is detected the orifice is reblown. We consistently find that the straightest orifices are produced by shrinking a larger diameter hole down to the proper size rather than by enlarging a hole which is too small. Nozzle diameters are typically 0.076 mm for oxygen–argon discharges and 0.191 mm when oxygen–helium mixtures are used. The reasons for using two differently sized nozzles will be covered in the next section of this paper. Nozzle assembly is then completed by attaching the coolant inlet and outlet arms to the water jacket and by briefly etching the inner quartz tube with a dilute solution of hydrofluoric acid. This acid rinse is believed to inhibit atomic recombination on the walls of the tube.[12]

B. Electrical design

Two distinct radio frequency circuit arrangements can be used for generating electrodeless discharges in gases.[13] One arrangement involves the use of a self-

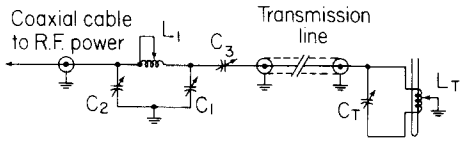

FIG. 3. Impedance matching circuitry.

excited power oscillator. In this configuration the tube containing the gas to be discharged is placed through the tank coil of a free-running power oscillator. Large amounts of radio frequency power can be coupled to a discharge in this manner, but it is inherently inefficient and can pull out of oscillation as the circuit loading changes. Loading variations can occur when the pressure of the discharge is varied over several hundred Torr. Its most serious drawback is that impedance matching between the plasma and the oscillator's circuitry, while the oscillator is in operation, is very difficult to achieve. The other circuit option, and the one which we have adopted, uses a driven oscillator–amplifier arrangement in which a variable frequency oscillator is separated from the load by one or more stages of amplification. In this manner the oscillator is very well isolated from load variations induced by changing plasma characteristics. More importantly, this arrangement allows the impedance of the gaseous discharge to be carefully matched to that of the radio frequency electronics. This ensures efficient use of the available radio frequency power. It also offers the desirable option of separating the electronics from the plasma coupling LC tank circuit.

The radio frequency (hereafter, rf) power for our beam source is supplied by a Viking Valiant radio transmitter which can deliver a maximum output of 140 W over a continuously variable frequency range several hundred kilohertz wide, centered at 14 MHz. (It is difficult to obtain wide frequency tunability in the coupling tank circuit of this beam source at frequencies significantly higher than 25 MHz due to the stray capacitance associated with its physical layout.) When higher power levels are required a linear amplifier capable of providing rf output levels of up to ca. 750 W is used. However, rf levels exceeding 200 W are rarely needed due to the highly efficient impedance matching scheme which is employed. The plasma coupling tank coil and capacitor can be seen in Fig. 1. The variable air capacitor (Bud #1615, 0–75 pF, 0.762 cm airgap) is mounted outside of the vacuum to facilitate the initial frequency matching of the coupling tank circuit to the electronics. A grid dip meter is used for this preliminary tuning of the beam source.

A novel impedance matching scheme is used which enables the source to operate routinely at a standing wave ratio (SWR) of less than 1.05 : 1. Impedance matching is necessary since the effective plasma impedance which varies as a function of plasma condition, is much larger than the 50-Ω output impedance of the electronics. Figure 3 shows a schematic outline of the impedance matching circuitry which can best be understood when viewed in two stages. First, a variable group tap on the tank coil (Fig. 2,A) is used to produce a large stepdown of the plasma impedance, as seen by the rf electronics, ideally to 50 Ω. This large stepdown of the plasma impedance is accomplished with the coupling coil-ground tap arrangement acting as an rf autotransformer. Since this is an rf circuit, the impedance transformation (for a uniformly wound coil) goes only approximately[14] as the square of the turns ratio, $(N/n)^2$, where N is the total number of coil turns and n is the numbers of turns from the rear of the coil to the ground tap. This impedance transformation creates a large voltage stepup at the front of the coil (nearest the nozzle tip) and necessitates the use of a high voltage ceramic feedthrough for the rf return, as is shown in Fig. 1,J. This large, but approximate impedance transformation allows the rf power to be delivered to the beam source from a remote location by RG-213/U coaxial cable. In a procedure which must be carried out only once when the source is first constructed, the source must be repeatedly teated with the position of the ground tap varied in order to determine optimum placement of the ground tap. This placement is found by noting the tap location which minimizes the standing wave ratio between the final rf amplification stage and the tank circuit. For the source geometry shown in Fig. 1 the optimum tap locations are 2¼ turns from the rear end of the coil for discharging oxygen–helium mixtures at 200 Torr, and 2½ turns from the rear end for oxygen–argon discharges operated at up to 350 Torr total pressure. Standing wave ratios are always less than 3 : 1 with these tap locations and are frequently much lower.

Next, a PI network, series capacitor arrangement is used to critically fine tune the impedance match until standing wave ratios of 1.1 : 1 or less are achieved. This circuit arrangement represents a quite diverse impedance matching scheme in that the PI-network can be used to match purely resistive load mismatches while the series capacitor can be used for tuning out any reactive impedance components presented to the rf electronics by the plasma coupling tank circuit. We find that the circuit impedance changes when the plasma is first started, varies rapidly as the nozzle pressure is raised from 1 to about 50 Torr, and then varies more slowly as the pressure is further raised to several hundred Torr. It is also found to vary with rf power level and gas composition. These impedance variations arise from the changing reactance of the coupling coil, which can be attributed to the changing permeability of the region inside the tank coil. In the original design and testing of this circuit a highly variable PI-network, series capacitor arrangement was constructed having an intended circuit Q of 10. The equations used for the design of the PI-network[15,16] were (for $R_1 > R_2$):

$$X_{C1} = R_1/Q, \tag{1}$$

$$X_{C2} = R_2\left(\frac{R_1/R_2}{Q^2 + 1 - (R_1/R_2)}\right)^{1/2}, \tag{2}$$

$$X_{L1} = \frac{QR_1 + (R_1R_2/X_{C2})}{Q^2 + 1}, \quad (3)$$

where X_{C1}, X_{C2}, and X_{L1} represent the reactances of the components shown in Fig. 3, R_1 and R_2 represent the impedances of the tank circuit and rf electronics, respectively, and Q is the quality factor of the matching network. Particular attention should be focused on R_1 in the above equations, noting that it is related to the stepped-down resistive impedance of the gaseous discharge. The series capacitor, C3 in Fig. 3, completes the impedance matching circuitry and is varied during the SWR minimization procedure in order to eliminate any reactive components of the tank circuit impedance. In the initial design of this circuit both C1 and C2 were variable up to 750 pF and were comprised of several high voltage ceramic and air variable capacitors which were connected in parallel. Also in the initial design, capacitor C3 was variable up to 250 pF while the inductor, L1, had a maximum calculated inductance of 6.9 μH. It consisted of a 7.6 cm diameter by 15.2 cm long, 15-turn tapped coil which was constructed out of 0.64-cm-diam copper tubing. The tap could be attached to the coil in 30 positions distributed evenly along the length of the coil, making L1 values well below 1 μH possible. This circuit worked very well but was eventually replaced (for ease of operation) by a slightly modified, commercially available network.[17] In this commercial unit C1 and C3 are 20–245 pF air variable capacitors, C2 is variable in discrete jumps up to 2160 pF, and L1 consists of a 5.1 cm diameter by 9.1 cm long, 9-turn coil which is tapped on its fifth turn for 14-MHz operation. The tuning of these impedance matching circuits is greatly facilitated by the continuous use of in-line rf wattmeters and a standing wave ratio bridge. Power coupling to the plasma is found to be extremely efficient ($\geq$99%) and power levels must be carefully limited in order to avoid melting the orifice of the quartz nozzle. Stray rf fields radiating from the source have been minimized by completely enclosing the top of the beam source with electrically grounded copper mesh.

Figure 4 shows a block diagram of the rf circuitry. Note that the beam source is always operated in a doubly interlocked condition. Nozzle meltdown protection is provided by a paddlewheel flow switch[18] which can quickly turn off the rf power should the nozzle coolant flow rate drop below a predetermined level. Similarly, the rf electronics are protected by a fast electronic meter relay which has been incorporated into an SWR bridge circuit. This relay can rapidly turn off the rf power when the SWR rises above some preset value, which is usually chosen as an SWR of 2.5 : 1.

Finally, we have been successful in localizing the plasma directly behind the orifice of the nozzle. This spatial localization of the plasma is of critical importance if an atomic beam of high molecular dissociation is to be produced from a high pressure discharge. Without this plasma localization at the nozzle tip extensive atomic recombination would occur. The localization has been

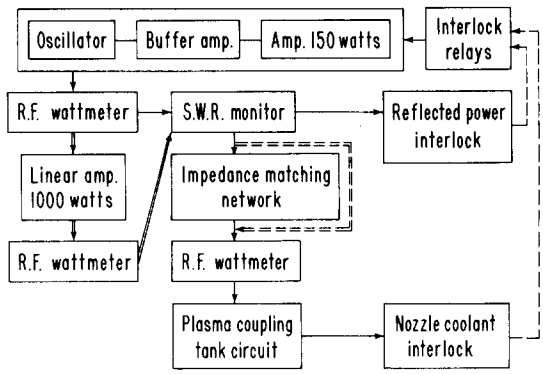

FIG. 4. Block diagram of the plasma generating electronics. The double solid lines indicate the equipment used for high power operation, while the double dashed lines indicate the bypassing necessary for preliminary tuneup of the source.

achieved by placing around the nozzle tip (outside of the water jacket and not along the front face of the nozzle) a carefully shaped, electrically grounded block of aluminum (Fig. 2,J). The discharge appears to change gradually from an inductively coupled plasma at low pressures to a capacitively coupled discharge at high pressures. This coupling at high pressures occurs between the front, small diameter tank coil turns, and the grounded aluminum block. As this coupling becomes stronger the plasma localizes towards the front of the discharge tube. Photographic studies have shown that the discharge region protrudes past the front plane of the grounding block and actually extends up to the nozzle tip, ensuring a high degree of molecular dissociation directly behind the nozzle at high pressures.

The tank coil (Fig. 2,D) has been differentially wound in order to further localize the plasma and to increase its energy density at high pressures. The first 6½ coil turns nearest to the nozzle tip are 1.37 cm i.d. by ~6.0 cm long while the 5 large turns are 5.08 cm i.d. by ~6.5 cm long. The larger turns decouple from the plasma as the pressure is raised, and therefore the energy density of the localized plasma is considerably increased. The coil is constructed of 0.32-cm-o.d. copper tubing and was wound around correctly sized metal tubes on a low-speed lathe. The small diameter coil windings should be uniformly spaced and carefully shaped in order to avoid any inhomogeneities in the rf field. These inhomogeneities, if present, can cause the uniform plasma to collapse into streamers at high pressures. The coil is water cooled with low electrical conductivity water at a flow rate of 4 cm^3/s in order to improve the long term mechanical, and hence electrical, stability of the tank circuit. Also note that the entire tank circuit, as seen in Fig. 1, is floated with respect to electrical ground. That is required if the rf coupling and localization schemes, as described here, are to be effectively used.

The pumping requirements for this beam source vary greatly depending upon the gas mixture which is to be used. It was originally pumped by a 4200-l/s diffusion pump which was separated from the source by a sliding

gate valve. This pumping arrangement was recently replaced by an 8000-l/s pump which was directly joined to the source. This large pumping speed is desirable while running high pressure oxygen–argon mixtures, for which the pressure must be kept below 7×10^{-5} Torr. For higher background pressures the rf power decouples from the nozzle and a glow discharge of the entire source region occurs. This glow discharge is a problem which currently constrains the nozzle orifice diameter to 0.075 mm for gas mixtures containing argon. Nozzle pressures exceeding 350 Torr have been successfully run with argon as the carrier gas. Helium seeded beams do not have this operational constraint. This allows much larger orifices to be used for helium seeded beams operating at high nozzle stagnation pressures, provided that sufficient pumping speed is available for backing the foreline of the diffusion pump.

Significant effort was also devoted to fabricating a skimmer which would not degrade when exposed to the atomic oxygen beam. Skimmers made of electrically conducting materials, including stainless steel, were not stable over long time periods due to sputtering by high energy ions. Apparently, ions emanating from the nozzle were being accelerated towards the ground potential of these metallic skimmers. Boron nitride[19] skimmers with 0.81-mm openings were found to be completely stable with respect to the oxygen beam. The electrical insulating properties, machinability, and density of boron nitride actually make it an ideal skimmer material for use with this beam source.

C. Source operation

The tuning and operating of the beam source is quite straightforward. The plasma coupling tank circuit should first be tuned to the desired resonant frequency by adjusting the tank circuit's variable air capacitor, which is mounted on top of the beam source. The resonant frequency of this circuit can be easily monitored by placing the probe of a grid dip meter adjacent to the tank circuit capacitor, which is conveniently located outside of the vacuum. During this tune-up procedure the coaxial cable which brings the rf power to the source should be disconnected from the source to ensure correct tuning of the circuit. Next, the rf power should be turned on ($\sim$100 W) with the impedance matching network and high power amplifier temporarily bypassed, and with the nozzle evacuated to $\lesssim$1 Torr. The variable frequency oscillator is then varied until the SWR between the beam source and the electronics is minimized. If the discharge is not ignited when the SWR minimum is reached the rf power should be quickly switched off and then on again. Invariably the discharge will be ignited by this procedure. Gas should now be introduced to the nozzle while simultaneously retuning the oscillator's frequency to maintain the SWR at a minimum. When pressures on the order of 100 Torr are reached, the rf power level may be safely increased to sustain the discharge at higher pressures. The pressure may then be further increased, again with the simultaneous retuning of the rf electronics, until the final operating pressure is reached. We consistently find that the resonant frequency of the plasma coupling circuit increases slowly with increasing gas pressure. As an example of this, a 5% O_2–He, 130-W discharge is found to require a 0.006 MHz frequency increase when its pressure is raised from 120 to 220 Torr. At this point the plasma should be switched off, the gas mixture in the beam source evacuated, and then the impedance matching circuitry along with any high power amplifiers inserted in-line. The source can now be reignited and tuned for optimum performance at high rf power levels. After a few minutes of operation at the final power and pressure settings the electronics should again be slightly retuned to correct for any drift during this initial stabilization period. It should be clearly stated here that the minimum SWR which can be achieved *before* the matching network is connected is completely dependent on the placement of the coupling coil's ground tap (Fig. 2,A). As was discussed earlier, the correct location for this tap must be found in a trial and error process which need be done only once when the source is initially constructed.

After the overall tuning procedure has been completed the source can be operated without further major retuning for a period lasting several weeks. Typically the source is turned on by evacuating the nozzle to about 1 Torr, switching on the rf power, and rapidly increasing the pressure to the desired operating level. Within a few minutes of reigniting the discharge the operating characteristics always return to their steady-state value. Most importantly, the beam characteristics are extremely reproducible for day to day operation of the source, allowing experimental scattering data to be taken over a period several weeks long if necessary, without concern for fluctuating beam characteristics. The quartz orifice does not enlarge at all when the source is operated at the power levels discussed in the next section of this paper. However, sputtering of the front surface of the quartz nozzle does place a limit on the lifetime of any given nozzle. This sputtering results when ions which leave the nozzle are accelerated back towards its front surface by the large rf fields present in that region. Periodic visual inspections of the nozzle tip are carried out to monitor the nozzle degradation. The nozzles are replaced when the sputtering erosion becomes severe. They can be recycled by rebuilding the nozzle face and reblowing the orifice. Some of the ions which emanate from the nozzle actually pass through the skimmer. These are deflected out of the beam by a 5000-V/cm deflecting field which is placed before the collision region of our apparatus (Fig. 1,N). The beam characteristics for different nozzles operated under the same conditions have been found to be fairly reproducible, with slight differences in Mach number and peak velocity being noted. These differences can be attributed to the slight coil shape and positioning changes which invariably occur during each reassembly of the beam source.

II. BEAM CHARACTERIZATION

A. Confirmation of atomic oxygen production

The atomic oxygen beams produced by this beam source have been thoroughly characterized in order to improve our understanding of the source's operation and to optimize its performance. A wide variety of diagnostic techniques have been used for this analysis. Chronologically, our first goal was to experimentally verify the presence of oxygen atoms in the terminal beam. This was unambiguously demonstrated by measuring the differential elastic scattering cross section for O–He and O_2–He in our universal crossed molecular beam apparatus.[20] In these measurements the elastically scattered mass 16 and mass 32 number densities were recorded, with the discharge on, when the oxygen beam was crossed at 90° with a supersonic beam of pure helium. For this preliminary experiment a 5% O_2–Ar mixture was discharged in the source at 95 Torr total pressure by 95 W of rf power. The Newton velocity diagrams[21] for these two collision systems are shown in Fig. 5(a), and clearly reveal how the presence of atomic oxygen in the terminal beam can be confirmed by these experiments. They show that the heavier molecular oxygen is kinematically constrained to scatter within a LAB angle of approximately 24° while the lighter atomic oxygen, if present in the beam, could be scattered to 44° in the LAB reference frame. These differential cross sections would also be expected to have a rather broad peak in the vicinity of these cutoff angles due to the nature of the transformation Jacobian which relates the LAB and center-of-mass reference frames. Figure 5(b) shows the experimentally measured differential elastic cross sections for these two systems. The mass 16 (O–He) scan can be seen in this figure to have a qualitatively different shape from the mass 32 (O_2–He) scan. This difference indicates that the mass 16 signal does not exclusively come from the dissociative ionization of elastically scattered molecular oxygen in the ionizer of our quadrupole mass spectrometer. More importantly, the mass 16 scan does in fact peak and begin to fall off around 40° while for the mass 32 scan this occurs at 20°, in excellent agreement with the shapes predicted from the most probable Newton diagrams shown in Fig. 5(a). The experimental curves actually extend past the predicted cutoff angles due to the finite spread of velocities in the two beams. The O–He experimental curve shown in Fig. 5(b) has been corrected for the dissociative ionization of elastically scattered molecular oxygen. We conclude from the above data that oxygen atoms are definitely present and, in fact, they are more abundant than oxygen molecules in the terminal beam produced by our high pressure, rf discharge beam source.

B. Molecular dissociation

The extent of O_2 dissociation in the terminal beam has been carefully measured for several oxygen-rare gas mixtures as a function of gas pressure and rf power.

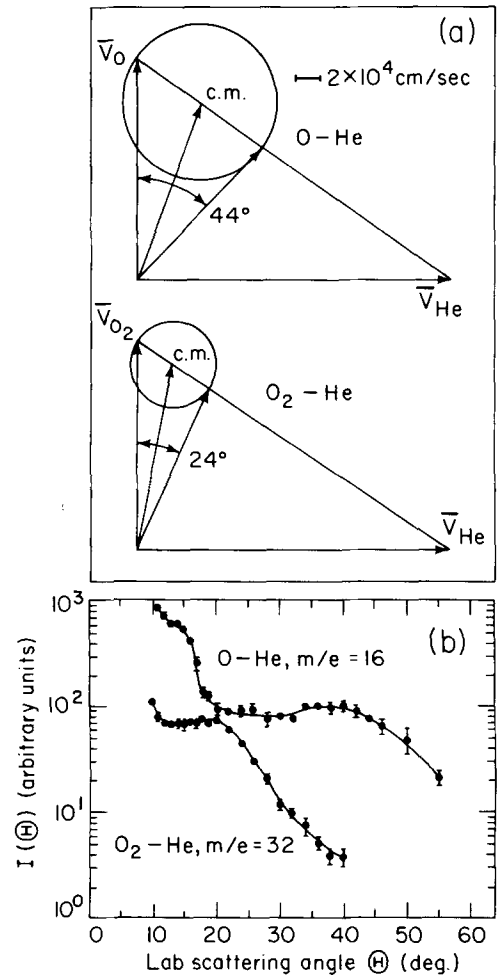

FIG. 5. (a) Newton diagrams for O–He and O_2–He elastic scattering. (b) Differential elastic scattering cross sections for O–He and O_2–He. The wide angle falloff of the O–He curve conclusively demonstrates atomic oxygen production.

These measurements were made in our crossed beam apparatus with the triply differentially pumped mass spectrometer looking directly along the beam axis. The relative O and O_2 number densities were actually measured by integrating the time-of-flight spectra of masses 16 and 32. We have opted to integrate these time-of-flight spectra rather than use our usual particle counting electronics in order to eliminate any possible contributions from VUV photons and high energy ions in the detected signals. This separation of the true signal from VUV photon and high energy ion contributions can easily be made in the time regime with our time-of-flight (hereafter, TOF) instrumentation since the interfering factors always have much shorter flight times than the true signal. The ion deflecting field mentioned earlier was held at a field strength of 5000 V/cm during these measurements and was found to deflect virtually all of the ions emanating from the beam source. Only during very high power operation of the beam source did a few high energy ions apparently reach the detector.

The TOF apparatus used in these studies consisted of a 17.78-cm-diam aluminum disk having four equally spaced 0.5 or 1.0 mm slots around its circumference. The disk was rotated at either 300 or 350 Hz during data

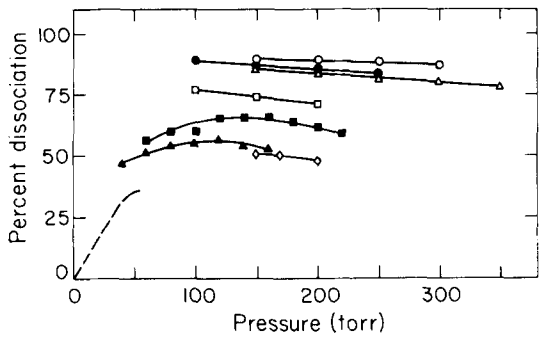

FIG. 6. Pressure dependence of O_2 dissociation: ○ 5% O_2–Ar, 165 W; ● 5% O_2–Ar, 130 W; △ 10% O_2–Ar, 195 W; □ 10% O_2–Ar, 140 W; ■ 5% O_2–He, 130 W; ▲ 10% O_2–He, 130 W; ◇ 10% O_2–He, 165 W; --- performance data for the source described in Ref. 8.

acquisition. The detector aperture was narrowed to 0.125 mm diameter, and the distance between the TOF disk and the electron bombardment ionizer was 18.4 cm. The ionizer and quadrupole mass spectrometer have been previously described in detail,[20] and the ionizer's emission current was set sufficiently low to eliminate any space charge perturbations of the detected signal intensities and velocity distributions. A 256-channel scaler interfaced to an on-line NOVA minicomputer was used to record signal intensity as a function of flight time. The scaler was usually set at 2-μs dwell time for the helium mixtures and 4 μs for the argon mixtures.

The extent of molecular dissociation in the terminal beam was calculated with the following two equations:

$$R = \frac{N_0}{N_{0_2}} = \frac{(\sigma_D/\sigma_{0_2})}{\eta}\left(\frac{\sigma_{0_2}}{\sigma_0}\right)\left(\frac{I_0 - \eta I_{0_2}}{I_{0_2}}\right), \quad (4)$$

$$\text{percent dissociation} = R/(R + 2), \quad (5)$$

where I_0 and I_{0_2} are the experimentally observed mass 16 and 32 number densities, η is the experimentally observed I_0/I_{0_2} count ratio with the discharge off, and the cross sections represent the following processes:

$$\sigma_{0_2} : O_2 + e \rightarrow O_2^+ + 2e,$$

$$\sigma_0 : O + e \rightarrow O^+ + 2e,$$

$$\sigma_D : O_2 + e \rightarrow O + O^+ + 2e.$$

For ionization with 250-eV electrons: $\sigma_{0_2} = 1.52$ A^2, $\sigma_0 = 1.15$ Å^2, and $\sigma_D = 0.88$ Å^2.[22,23] In their paper Miller and Patch[8] have used an equivalent expression for R, and have discussed the approximations and assumptions leading to the use of Eqs. (4) and (5). The $(\sigma_D/\sigma_{0_2})/\eta$ term corrects for any differential detection of masses 16 and 32 by our detector. This difference in detection probability, if present at all, is partially due to the differential transmission of m/e = 16 and 32 through the quadrupole mass filter of our detector.

Figure 6 shows the pressure dependence of O_2 dissociation for four oxygen–rare gas mixtures under a variety of rf power settings. These curves reveal the unique operating characteristics of this beam source. The molecular dissociation is seen to depend only weakly on the nozzle stagnation pressure, varying only a few percent over a several hundred Torr pressure range. The actual extent of molecular dissociation in the beam is also found to be quite high over this large pressure range. Argon seeded mixtures regularly achieve molecular dissociation levels of 80%–90% while helium seeded mixtures operate with 50%–65% dissociation. The weak pressure dependence and high dissociation levels described here can undoubtedly be attributed to the spatial localization of the plasma at the tip of the quartz nozzle. The dissociation percentages shown in Fig. 6 have been found to be reproducible to within about 5% for data taken over a several month time period with many different nozzles. Further examination of the curves shown in Fig. 6 indicates that the dissociation versus pressure curves for identical gas mixtures discharged by different rf power levels have similar slopes, with the higher power curves shifted to slightly greater dissociation. The 10% oxygen mixtures also appear to exhibit slightly lower dissociation values than their more dilute counterparts.

Figure 7 shows even more clearly the effect of rf power and O_2 concentration on molecular dissociation. Increasing the rf power from 130 to 195 W is seen to raise the dissociation level by at most 10% for three different gas mixtures. The two upper curves of this figure also show that the extent of molecular dissociation is only mildly influenced by raising the O_2 concentration from 5% to 10% when argon is used as the carrier gas. The 10% O_2–Ar mixture is seen from Fig. 7 to exhibit the same rf power dependence as the 5% O_2–Ar mixture, with its dissociation percentage lower by about 10%.

The information related in Figs. 6 and 7 has been very useful for optimizing the performance of our oxygen atom beam source. The very weak pressure dependences shown in Fig. 6 indicate that the nozzle stagnation pressure should be held as high as possible, subject to the limitations of plasma stability and pumping speed availability, without worry of severe recombination. These figures also tell us that 10% O_2–rare gas mixtures should be used rather than more dilute mixtures in order to increase the flux of oxygen atoms leaving the nozzle.

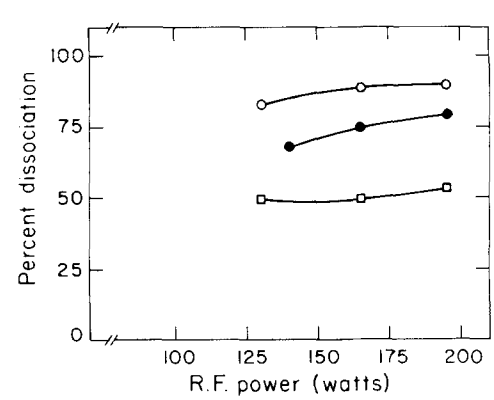

FIG. 7. The rf power dependence of O_2 dissociation: ○ 5% O_2–Ar, 250 Torr; ● 10% O_2–Ar, 250 Torr; □ 10% O_2–He, 175 Torr.

Finally, Fig. 7 informs us that power levels approaching 200 W should be quite adequate for dissociating molecular oxygen in seeded argon and helium gas mixtures. This is fortunate since power levels exceeding 200 W lead to orifice enlargement when argon is used as the carrier gas. Power levels exceeding 200 W also appear to accelerate the quartz sputtering rate at the nozzle face for all gas mixtures tested.

C. Velocity analysis

The true, undistorted atomic oxygen velocity distributions produced by our beam source have been recovered from the convoluted experimental TOF distributions by correcting the observed spectra for instrumental broadening effects (shutter function and finite ionizer length) and ion flight time offset. The peak velocity and Mach number of these distributions have been found to vary with both nozzle stagnation pressure and rf power level. Figure 8 indicates the dependence of peak velocity on nozzle pressure for seven different gas mixture–rf power combinations. The effect of seeding is immediately apparent here, with the oxygen seeded in helium beams having much higher velocities than the oxygen seeded in argon gas mixtures. The mean energy of the atomic oxygen beams generated in our laboratory spanned the range from 0.1–0.5 eV, with the highest energies being obtained for 5% O_2–He mixtures discharged with 200 W. The shape of the curves shown in Fig. 8 indicates that velocity "slippage" occurs between the oxygen and carrier gases during the hydrodynamic nozzle expansion. Velocity slippage occurs when the collision frequency is too low during the nozzle expansion to effect complete momentum and energy equilibrium between the seed and carrier species. Slippage is especially typical of low pressure, high temperature expansions due to the relatively low number density these systems have in the vicinity of the nozzle orifice. When slippage occurs it can usually be minimized by increasing the pressure behind the nozzle, which increases the number of collisions which occur during the expansion. This behavior is clearly seen in Fig. 8.

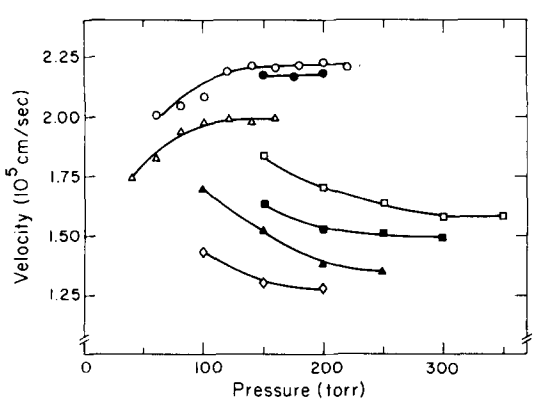

FIG. 8. Pressure dependence of atomic beam velocity: ○ 5% O_2–He, 130 W; ● 10% O_2–He, 165 W; △ 10% O_2–He, 130 W; □ 10% O_2–Ar, 195 W; ■ 5% O_2–Ar, 165 W; ▲ 5% O_2–Ar, 130 W; ◇ 10% O_2–Ar, 140 W.

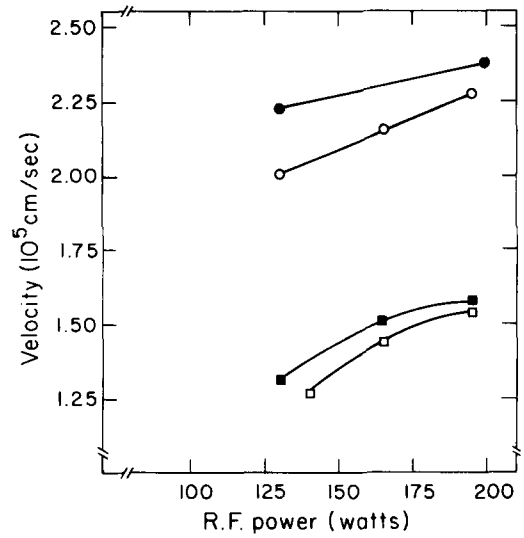

FIG. 9. The rf power dependence of atomic beam velocity: ● 5% O_2–He, 200 Torr; ○ 10% O_2–He, 175 Torr; ■ 5% O_2–Ar, 250 Torr; □ 10% O_2–Ar, 250 Torr.

The mixtures having helium as the carrier gas have their atomic oxygen peak velocities steadily *increasing* with increasing pressure until their terminal velocities are reached at pressures approaching 150–200 Torr. The mixtures having argon as the carrier gas behave oppositely from this, with their peak oxygen velocities *decreasing* with increasing pressure until their terminal velocities are reached between 250 and 300 Torr. The above behavior is expected since helium serves to accelerate atomic oxygen while argon decelerates atomic oxygen during coexpansion from the nozzle.

The influence of rf power on beam velocity has also been studied and is shown in Fig. 9 for four gas mixtures. In all cases the atomic oxygen velocity is found to increase monotonically with increasing rf power. This in turn indicates that the effective plasma temperature does in fact rise with increasing rf power. The translational energy of the beam can therefore be tuned over a narrow energy range about 0.1 eV wide by simply varying the rf power used to run the discharge. This tunability may apply to an even broader energy range when power levels exceeding 200 W are used for running oxygen–helium mixtures.

In these experiments the raw TOF data is always recorded as number density versus flight time. However, TOF spectra are more readily interpretable when displayed as flux versus velocity spectra. A typical TOF spectra is shown in Fig. 10 which represents the velocity distribution of a fast atomic oxygen beam. The correct Jacobian transformation $1/v^2$ was used for converting this and other spectra from time space to velocity space, while the resulting distributions were then multiplied by v to effect the conversion from number density to flux. The oxygen seeded in helium distribution shown in Fig. 10 has a FWHM of 19% with a Mach number of 9.2 as calculated by a parametric fit to the deconvoluted distribution.[24,25] This should be compared to the width of an effusive beam whose velocity distribution is Max-

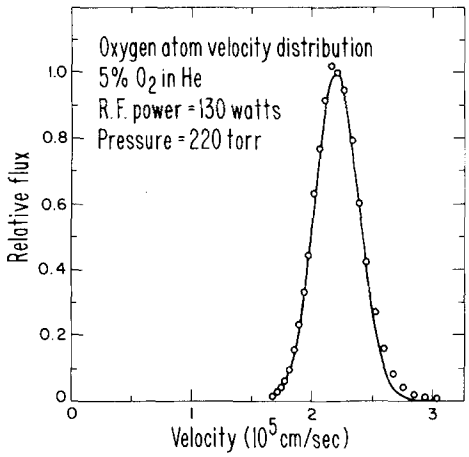

FIG. 10. Atomic oxygen velocity distribution for a seeded beam having a FWHM of 19%. The solid line is the deconvoluted best fit to the experimental data which yields a beam Mach number of 9.2.

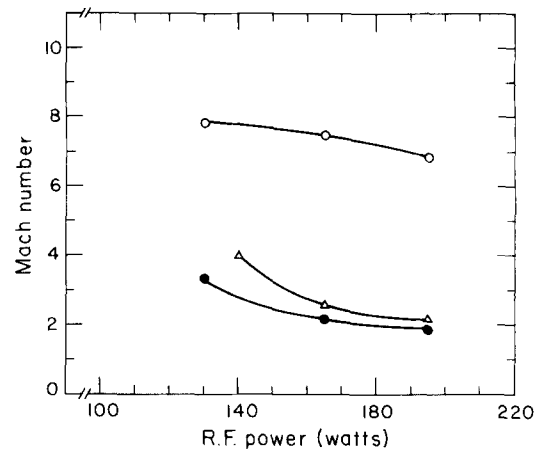

FIG. 12. The rf power dependence of atomic beam Mach number: ○ 10% O_2–He, 175 Torr; △ 10% O_2–Ar, 250 Torr; ● 5% O_2–Ar, 250 Torr.

wellian. Numerical solution of the transcendental equation which defines the two half-intensity velocities of the distribution $I(v) \propto v_3 \exp(-v^2/\alpha^2)$ shows that the FWHM of a Maxwellian flux distribution is ~95%. The relatively narrow velocity distributions produced by this beam source are one of its most important characteristics, and are in general indicative of beams produced from supersonic nozzle expansions. The slower oxygen seeded in argon beams have typically ~40% FWHM distributions with Mach numbers ranging from 3 to 4. In the future the use of neon rather than argon as the beam carrier gas may enable narrower moderate energy beams to be produced due to the smaller mass mismatch which exists between neon and atomic oxygen relative to that of argon.

The terminal Mach number of a beam is a parameter which is frequently used for characterizing the width of its velocity distribution. It is defined as the ratio of the mass flow speed to the local speed of sound in the beam, v/c, where $c = (\gamma k T_b/m)^{1/2}$, γ is the usual ratio of specific heats at constant pressure to constant volume, and T_b is the temperature of the beam in the reference frame moving with the bulk velocity v. For seeded gas mixtures which are expanded in the hydrodynamic regime (Knudsen number < 1) collisions with the carrier gas initially accelerate or decelerate the seed gas depending on whether the carrier gas is lighter or heavier than the seed gas, respectively. Subsequent collisions during the expansion then serve to "cool" the seed gas and to narrow the width of its velocity distribution.[26] The total number of binary collisions which occur during the expansion is proportional to $n_0 D$, the product of the particle number density at the orifice with the orifice diameter. Figures 11 and 12 show how the atomic oxygen Mach number varies respectively with nozzle stagnation pressure and rf power for several operating conditions of the beam source. The nearly linear Mach number versus pressure curves shown in Fig. 11 indicate that the cooling process does vary as described above, and is not complete. It is clear from the slope of the curves shown in Fig. 11 that further velocity distribution narrowing should be possible for operation at still higher stagnation pressures. This statement particularly applies to helium containing mixtures, where the additon of a Roots blower to our pumping system will enable the source to operate with higher nozzle pressures (or with a larger nozzle orifice, which would also increase the terminal Mach number of the beam). Figure 12 shows that the beam Mach number decreases as a function of rf power level. This is not surprising since the number density at the orifice decreases as $1/T$, where T is the effective plasma temperature at the orifice. It is nevertheless important to understand the actual *extent* of Mach number degradation with increasing rf power since future operation of the beam source at higher stagnation pressures may require the use of higher power levels.

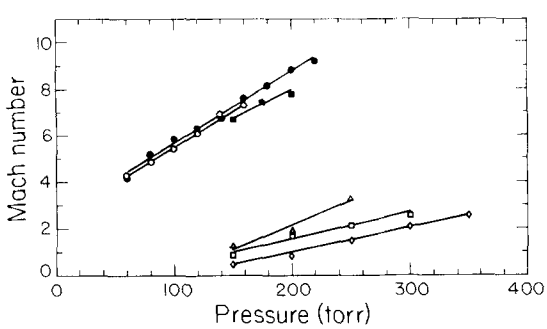

FIG. 11. Pressure dependence of atomic beam Mach number: ● 5% O_2–He, 130 W; ○ 10% O_2–He, 130 W; ◇ 10% O_2–Ar, 195 W; △ 5% O_2–Ar, 130 W; □ 5% O_2–Ar, 165 W; ■ 10% O_2–He, 165 W.

D. Plasma temperature

The temperature of the gas at the nozzle orifice has been determined for a variety of source operating conditions with two different techniques. The first of these techniques depends on the flux change which occurs when the gas temperature at the orifice is varied. The flux emanating from the orifice at constant stagnation pressure depends on the gas temperature in the following way:

$$\Phi(T) \propto n(T) \cdot v(T) \propto 1/\sqrt{T}, \tag{6}$$

where the particle number density, $n(T)$, varies as $1/T$ and the velocity of the particles emanating from the nozzle, $v(T)$, goes as $\sqrt{T}$. An approximate determination of the plasma temperature can therefore be made by measuring the pressure in the source with the discharge turned on and off:

$$\frac{P_1}{P_2} \propto \frac{\Phi_1}{\Phi_2} \propto \sqrt{\frac{T_2}{T_1}}. \tag{7}$$

A Bayard–Alpert ionization gauge was used for making these pressure measurements, and the gas temperature with the discharge off was assumed to be 300 K. Using Eq. (7) the plasma temperature for high pressure oxygen–helium mixtures is repeatedly found to range from 800–900 K for 130-W discharges, 850–1100 K for 165 W, and from 1150–1300 K for 195 W. Only a slight pressure dependence is observed, with the temperature tending to decrease slowly with increasing pressure. Oxygen–argon mixtures are found to be considerably hotter: 1300–1500 K for 130 W, 1600–1750 K for 165 W, and 1750–2050 K for 195 W discharges at high pressures. The oxygen–argon discharges also have much stronger pressure dependences than the oxygen–helium discharges, with their temperatures rising significantly as the stagnation pressure is lowered. As a specific example of this a 5% O_2–Ar, 130 W discharge was found to increase in temperature from 1400 to 1750 K as the pressure was lowered from 250 to 100 Torr. For this reason extreme caution should be taken when igniting (at low pressures) high power argon discharges. Immediately after igniting high power argon discharges the pressure should be quickly raised to at least 100 Torr in order to avoid melting of the quartz orifice. The above temperature measurements are of course only approximate, but are very useful for day to day plasma characterization. Also note that the electron temperatures in the plasma are much hotter than the above translational temperatures, with electron temperatures on the order of 10 000 K or higher being achieved in the discharge.

More accurate plasma temperature determinations can be made by monitoring the mole fractions and velocity distributions of the three species (O, O_2, and either helium or argon) which are present in the beam. These temperature determinations may be carried out by assuming the overall energy balance.[27,28]

$$(\Sigma X_i C_{P_i}) T_0 = \Sigma X_i C_{P_i} T_{bi} + \tfrac{1}{2} \Sigma X_i m_i v_i^2, \tag{8}$$

where X_i is the mole fraction, C_{P_i} the heat capacity, v_i the terminal velocity, m_i the mass, and T_{bi} the terminal temperature of each component of the beam, and T_0 is the temperature of the gas at the orifice. The assumptions which must be made in order to calculate T_0 from Eq. (8) have been thoroughly reviewed in Ref. 8. The mole fractions of each component have been calculated using the molecular dissociation data which was discussed earlier, taken in conjunction with the known composition of the gas mixture under investigation. Figure 13 shows the rf power dependence of gas temperature, at constant pressure, for three different gas mixtures. Once again we see that the argon containing mixtures generate significantly hotter plasmas and exhibit stronger power dependences than the helium containing ones. The data used in constructing these curves were intentionally taken at relatively high operating pressures in order to ensure the validity of Eq. (8). The pressure dependence of gas temperature, at constant rf power, has also been studied for several gas mixtures under a wide variety of operating conditions. These studies again indicate that the gas temperature decreases with increasing pressure. For example, helium containing gas mixtures typically decreased 200 degrees, from about 1000 to 800 K, for a pressure change from 100 to 200 Torr. Argon containing mixtures also exhibit this temperature decrease with increasing gas pressure. We also find that the assumptions which enable Eq. (8) to be used for calculating gas temperature appear to break down at low pressures for argon containing mixtures due to the poor quality of these expansions. This statement especially applies to high power, low pressure discharges which contain argon.

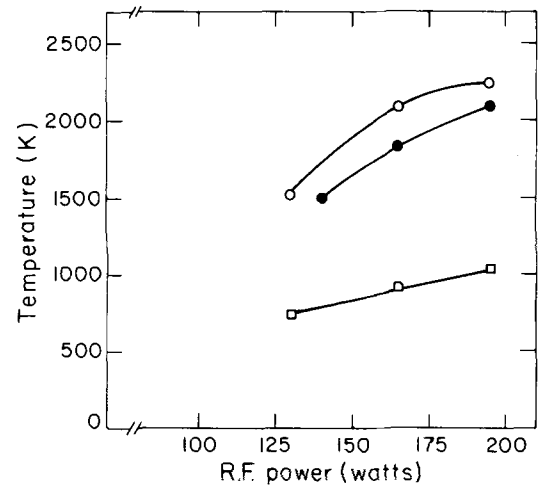

FIG. 13. The rf power dependence of plasma temperature: ○ 5% O_2–Ar, 250 Torr; ● 10% O_2–Ar, 250 Torr; □ 10% O_2–He, 175 Torr.

In a final attempt to gauge the true gas temperature at the orifice we have also measured the velocity distribution of a pure helium beam which was produced from a 200-Torr, 175-W discharge. Its peak velocity was found to be 2.83×10^5 cm/s. For an ideal nozzle expansion of a rare gas, where $v = (5kT_0/m)^{1/2}$, this velocity corresponds to a gas temperature of 770 K. This temperature can be considered to be in fairly good agreement with the temperatures determined above when we take into consideration the difference in gas composition which exists between this discharge and those previously discussed.

In concluding this section on plasma temperature characterization it should be mentioned that we have encountered some plasmas which were not suitable for generating atomic species. In particular, we have been unable to generate "hot" discharges for gas mixtures predominantly composed of helium when small nozzle orifices of ≤ 0.127 mm diameter were tested. These

"cool" discharges would typically have temperatures on the order of only 400 K for power levels up to 200 W. These "cool" discharges are fortunately of little practical concern since orifices of ≥0.180 mm diameter are always used for running helium containing mixtures. The rate of gas flow out of the orifice is therefore seen to influence the mode stability of discharges containing helium, with faster flow rates stabilizing the hotter mode (~1000 K) relative to the cooler mode (~400 K). Argon containing plasmas also have various discharge modes, with the two most important modes being the desired "hot mode" (~1750 K) and the destructive "streamer" or "pencil" mode which can occur for operation at pressures in excess of 400–500 Torr at high power levels. This latter mode is extremely hot and can cause rapid enlargement of the orifice. The inner diameter of the plasma containing quartz tube can influence the probability of this "hot mode" to "streamer mode" transition. The inner tube dimensions given earlier in this paper were chosen as a compromise between maximizing power coupling to the discharge and minimizing the probability of streamer formation at high pressures.

E. Beam intensity

Absolute beam flux measurements have been carried out in a differentially pumped beam source test facility in which a Bayard–Alpert gauge having a 52-cm sidearm extension was used as the particle detector. For these measurements the long sidearm of the detector gauge was pointed directly into the beam and was terminated with a small 1.58 mm conical aperture. The pressure rise ΔP, which is registered by the gauge when the beam is turned on, can be used for calculating the absolute intensity of the beam when the distance between the source skimmer and the detector entrance aperture d is accurately known. This intensity determination is possible since the pressure rise, ΔP, reflects the new rate equilibrium which is established between molecules entering the detector and those effusing from it. The rate at which molecules enter the detector can therefore be found by calculating the rate at which molecules effuse out of the detector. This effusion rate can be expressed as: $\Phi = \frac{1}{4} n_0 v_0 A$, where $n_0 = \Delta P/RT$, $v_0 = (8kT/\pi m)^{1/2}$, A is the area of the detector entrance aperture, and T is assumed to be 300 K. The long sidearm extension was added to the ionization gauge to ensure the validity of this last assumption. The absolute intensity of the beam in terms of solid angle units can be obtained by dividing Φ by $\Delta\Omega$, the solid angle subtended by the detector aperture, where $\Delta\Omega = A/d^2$. Examination of the above relationships reveals that the actual area of the detector aperture does not influence the outcome of the beam intensity determination as it cancels out in the final step of the calculation. The detector-skimmer distance d was fixed at 86.54 mm for these studies. Pure argon discharges which were operated at power levels between 165 and 195 W at stagnation pressures up to 350 Torr were found to have beam fluxes of 3.6×10^{18} atoms sr^{-1} s^{-1}. The atomic oxygen mole fraction present in the terminal beam of 10% O_2–Ar discharges, run under the same power and pressure settings as above, is known to be 0.15 from molecular dissociation experiments. By combining the above data the absolute oxygen atom flux produced by discharging oxygen–argon mixtures is found to be ca. 5×10^{17} atoms sr^{-1} s^{-1}. Pure helium discharges which were run at 200 Torr with power levels again between 165 and 195 W produced beam fluxes of 5.5×10^{19} atoms sr^{-1} s^{-1}. Combining this figure with the measured atomic oxygen mole fraction for 10% O_2–He discharges, $X = 0.10$, leads to an absolute atomic oxygen flux of ca. 5×10^{18} atoms sr^{-1} s^{-1} for oxygen–helium discharges. The pure rare gas beam intensities produced by this source, as described above, are comparable in magnitude to the intensities which have been reported in the literature for other nozzle beam sources.[29,30] The ionization gauge readings which were used for these and subsequent beam intensity calculations were corrected for the differences in gauge sensitivity which exist for the various gases under study. The gauge readings were actually divided by 1.19, 0.15, and 0.85 in order to find the true pressure changes due to Ar, He, and O_2, respectively.[31] These represent the correct gauge sensitivity conversion factors as the detector gauge was calibrated for N_2.

The pressure rises due to oxygen–rare gas beams were also measured in order to perform an approximate check on the atomic oxygen flux estimates described above. Predictions for the seeded beam pressure rises were based on the pure rare gas data, and were calculated in the following way: $\Delta P_{mix}(\text{predicted}) = [X_{RG} + X_{O_2} \times (0.85/S)]\Delta P_{RG}$, where X_{RG} and X_{O_2} represent the rare gas and oxygen concentrations of the gas mixture, ΔP_{RG} is the pressure rise registered by the gauge for a pure rare gas beam run under the same stagnation pressure and rf power settings, ΔP_{mix} is the predicted gauge pressure rise due to the seeded beam, and S is the gauge sensitivity conversion factor for either helium or argon. The measured gauge pressure increases for oxygen–argon discharges agreed well with the predicted gauge deflections, falling consistently within 10% of ΔP_{mix}. However, the measured pressure rises for oxygen–helium beams were usually 20% higher than the predicted gauge deflection. This discrepancy can be explained if the mole fraction of oxygen (O and O_2) along the beam axis is larger in the terminal beam than in the initial gas mixture. This explanation is supported by the fact that the heavier particles of a seeded gas mixture are preferentially focused on the beam centerline during hydrodynamic nozzle expansion,[32] and are attenuated less than lighter particles in the region between the nozzle orifice and the skimmer. In summary, we therefore find the atomic oxygen flux to be about 5×10^{17} atoms sr^{-1} s^{-1} for oxygen seeded in argon beams and $\geq 5 \times 10^{18}$ atoms sr^{-1} s^{-1} for oxygen seeded in helium beams. For these determinations a 40° inner–60° outer cone angle, 0.82-mm diameter boron nitride skimmer was fixed at a nozzle-skimmer distance of 5.08 mm, a second collimat-

ing skimmer of 1.04 mm diameter was placed 31.78 mm from the orifice, and a flat slot of variable dimensions was placed 52.76 mm from the orifice in the wall which separated the differential and detector sections of the apparatus. The total gas flow emanating from the nozzle is typically 0.75 Torr l/s for 200-Torr, 165–195 W oxygen–helium discharges (0.191-mm-diam orifice) and 0.25 Torr l/s for 350-Torr, 165–195 W oxygen–argon discharges (0.076-mm-diam orifice).

The ability of this beam source to produce intense atomic oxygen beams at high pressures, without suffering significant intensity loss due to atomic recombination, is one of its most novel and important operating characteristics. This behavior is clearly demonstrated in Fig. 14 where the atomic oxygen number density, as measured with a quadrupole mass spectrometer, is plotted as a function of increasing stagnation pressure for four gas mixture–rf power level combinations. In Fig. 14(a) the relative $m/e = 16$ number density is seen to rise linearly with increasing stagnation pressure over the entire pressure regimes which were explored for two argon containing gas mixtures: up to 300 Torr for a 5% O_2–Ar, 165 W discharge and 350 Torr for a 10% O_2–Ar, 195 W discharge. The 10% O_2–He, 165 W number density curve shown in Fig. 14(b) behaves in a similar manner, up to a maximum pressure of 200 Torr, as those described above. However, the 5% O_2–He, 130 W curve shown in this figure turns over at pressures higher than 200 Torr. This indicates that power levels $\geq$165 W should always be used for running oxygen–helium discharges above 200 Torr total pressure. The $m/e = 16$ curves shown in Fig. 14 have all been corrected for the slight contributions arising from dissociative ionization of the molecular oxygen which is present in the beam. The high pressure segments of these curves are also representative of the relative atomic oxygen *fluxes* produced by this source, as a function of increasing pressure, due to the weak dependence beam velocity has on gas pressure at high stagnation pressure.

F. $O(^1D_2)$ production

When dilute oxygen–helium gas mixtures are discharged in this beam source a mixture of atomic oxygen quantum states including ground state $O(^3P_J)$ and excited state $O(^1D_2)$ atoms is present in the terminal beam. When helium is used as the carrier gas the $O(^1D_2)$ flux has in fact proven to be of sufficient magnitude to permit differential reactive scattering experiments to be carried out. This represents a significant development in the realm of molecular beam technology as prior to this no other $O(^1D_2)$ beam source has been reported in the literature.

The $O(^1D_2)$ production was experimentally confirmed in our universal crossed molecular beam apparatus by observing the production of OH from the reaction

$$O(^1D_2) + H_2 \rightarrow OH + H$$
$$\Delta H = -43.5 \text{ kcal/mole.} \quad (9)$$

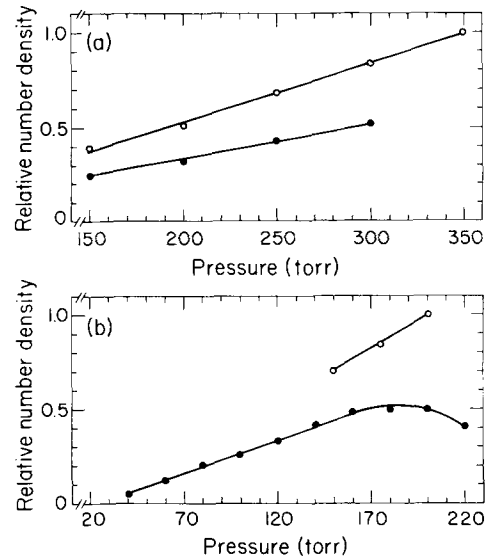

FIG. 14. (a) Atomic oxygen number density as a function of pressure for argon containing mixtures: ○ 10% O_2–Ar, 195 W; ● 5% O_2–Ar, 165 W. (b) Atomic oxygen number density as a function of pressure for helium containing mixtures: ○ 10% O_2–He, 165 W; ● 5% O_2–He, 130 W. These curves have all been corrected for slight $m/e = 16$ contributions arising from dissociative ionization of mass 32 in the electron bombardment ionizer.

For this study a supersonic hydrogen beam (peak velocity = 2.66×10^5 cm/s, Mach number = 21) was collided at 90° with an oxygen seeded in helium beam (peak atomic oxygen velocity = 2.38×10^5 cm/s, Mach number = 9) at a relative collision energy of 2.7 kcal/mole. The oxygen beam was produced by discharging a 200 Torr, 5% O_2–He gas mixture with 200 W of rf power. Under these experimental conditions the OH could not have been produced by the ground state reaction

$$O(^3P_J) + H_2 \rightarrow OH + H$$
$$\Delta H = 1.9 \text{ kcal/mole} \quad (10)$$

due to the large 8.9 kcal/mole activation energy[33] which is associated with this process. Further support of the reaction (9) process comes from the angular and velocity distributions of the OH reaction product. The OH LAB angular distribution shown in Fig. 15 extends as far as the $OH(v = 0)$ center-of-mass velocity circle permits based upon a reaction exoergicity of 43.5 kcal/mole, while the OH velocity distributions obtained with cross correlation time-of-flight techniques[34,35] fall off with velocities indicative of this exoergicity. These experimental distributions also indicate that the concentration of $O(^1S_0)$ atoms in the terminal beam must be extremely low as no OH product was observed at the high energies characteristic of the process

$$O(^1S_0) + H_2 \rightarrow OH + H$$
$$\Delta H = -94.7 \text{ kcal/mole.} \quad (11)$$

When 10% O_2–He gas mixtures were discharged rather than 5% O_2–He mixtures a 30% decrease in OH signal was observed relative to the 3000 counts/s counting rate of the more dilute mixture. This indicates that the num-

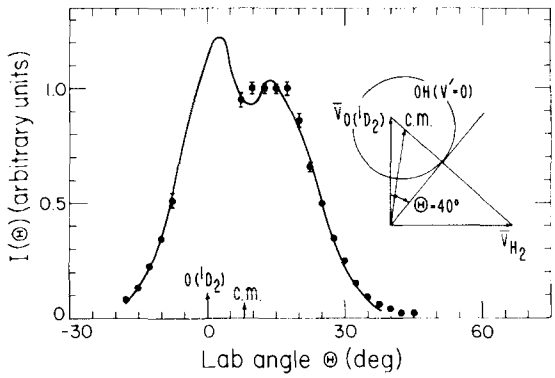

FIG. 15. Laboratory angular distribution of OH from the reaction $O(^1D_2) + H_2 \rightarrow OH + H$ at a relative collision energy of 2.7 kcal/mole. The solid line is a calculated fit to the experimental data which employed a symmetrical center-of-mass product distribution for the OH product. The excellent fit between the calculated and experimental data, taken in conjunction with wide angle falloff (~40°) of the distribution, demonstrates the presence of $O(^1D_2)$ atomic oxygen in the terminal beam.

ber of collisions occurring between $O(^1D_2)$ atoms and other oxygen species should be minimized during the expansion if extensive quenching of the $O(^1D_2)$ is to be avoided. When dilute oxygen–argon gas mixtures were tested no OH product was detected, indicating that, within the accuracy of the determination, oxygen seeded in argon beams contain no $O(^1D_2)$. This is fortunate as it enables $O(^3P_J)$ reactions to be studied in an environment free of $O(^1D_2)$ contamination when argon is used as the beam carrier gas.

The presence of $O(^1D_2)$ in beams having helium as the carrier gas can be attributed to the extremely small quenching rate constant of the process

$$O(^1D_2) + He(^1S_0) \rightarrow O(^3P_J) + He(^1S_0)$$
$$\Delta H = -45.4 \text{ kcal/mole}, \qquad (12)$$

which has been experimentally found to be: $k_{O-He}{}^{Q} < 10^{-16}$ cm^3 molecule^{-1} s^{-1}.[36] This value can be compared to the "gas kinetic" rate constant in order to crudely estimate the number of collisions needed for quenching to occur: $k_{O-He}{}^{GK} \approx 8 \times 10^{-10}$ cm^3 molecule^{-1} s^{-1}. This gas kinetic rate constant was approximated by $k^{GK} = (\pi r_m{}^2)(8kT/\pi\mu)^{1/2}$, where r_m is the experimentally determined Lennard-Jones (12,6) parameter for $O(^3P_J)$–He collisions,[37] T is the plasma temperature, taken as 1000 K, and μ is the reduced mass of the collision partners. The above indicates that, on the average, about 10^6 $O(^1D_2)$–He collisions must occur before quenching takes place. Since only about 10^2 collisions occur during the expansion[38] it is not surprising that some $O(^1D_2)$ atoms are present in the terminal beam. In fact, most $O(^1D_2)$ quenching probably occurs during collisions between $O(^1D_2)$ and other oxygen species which are present in the beam. In contrast to this, the experimentally determined rate constant for $O(^1D_2)$ quenching by Ar, $k_{O-Ar}{}^{Q} = 3 \times 10^{-13}$ cm^3 molecule^{-1} s^{-1},[36] is only about three orders of magnitude smaller than the O–Ar "gas kinetic" rate constant, $k_{O-Ar}{}^{GK} \approx 6 \times 10^{-10}$ cm^3 molecule^{-1} s^{-1}, which was calculated assuming a plasma temperature of 1500 K and using the r_m value for $O(^3P_J)$–Ar given by Ref. 37. The $O(^1D_2)$–Ar collisions therefore deactivate a significant fraction of the $O(^1D_2)$ atoms during expansion, with the remaining $O(^1D_2)$ atoms being deactivated by collision with the other atomic and molecular oxygen species which are present in the beam ($k_{O-O_2}{}^{Q} = 3.7 \times 10^{-11}$ cm^2 molecule^{-1} s^{-1}).[36] An analysis of the collision dynamics for Reaction (9) is currently being prepared for publication, and will be presented elsewhere in the literature.

The pressure and power dependence of $O(^1D_2)$ production has been examined for a 5% O_2–He gas mixture in our crossed beam apparatus. This was accomplished by monitoring, at the peak of the broad product angular distribution, the OH signal intensity coming from Reaction (9) as a function of beam source pressure and rf power level. Since the oxygen and hydrogen beam velocities are nearly equal the OH count rate is indicative of the $O(^1D_2)$ particle flux. (Whereas if the hydrogen beam were much faster than the oxygen beam the OH count rate would be indicative of the $O(^1D_2)$ number density at the collision center.) The curved shape of the intensity versus pressure data shown in Fig. 16(a) indicates that some $O(^1D_2)$ quenching does occur at higher pressures, but not to the extent which would require operating the sources at pressures below 250 Torr. The intensity versus rf power curves shown in Fig. 16(b) clearly indicate that higher source powers (and hence plasma temperatures) significantly increase

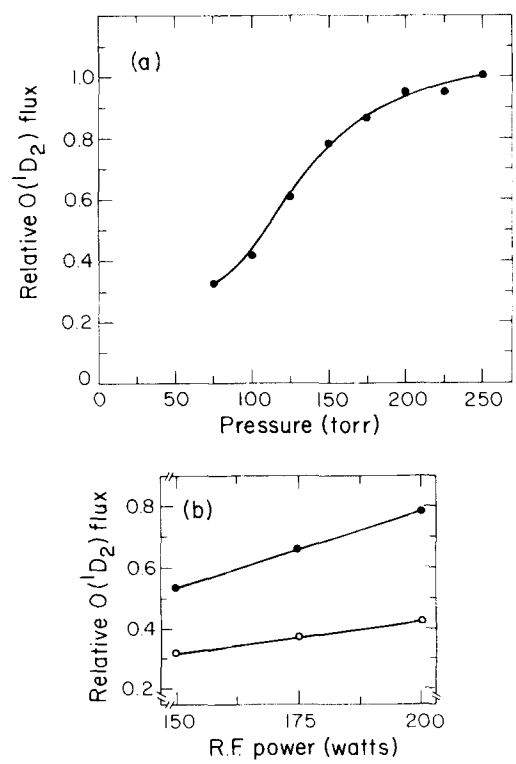

FIG. 16. (a) Relative $O(^1D_2)$ intensity as a function of gas pressure for a 5% O_2–He, 200 W discharge. (b) Relative $O(^1D_2)$ intensity as a function of rf power level for a 5% O_2–He gas mixture. ● 150 Torr total pressure; ○ 100 Torr total pressure. These curves indicate that the $O(^1D_2)$ intensity can be optimized by simultaneously operating the source at high power and pressure settings.

the flux of $O(^1D_2)$ emanating from the nozzle. In the near future gas mixtures composed of less than 5% oxygen will be characterized in order to determine the optimum oxygen–helium mixture for maximizing $O(^1D_2)$ production.

III. DISCUSSION

The high pressure, supersonic, radio frequency discharge beam source which has been described in the preceeding sections of this paper offers several improvements in the important operating characteristics of beam translational energy, beam intensity, velocity distribution width, and beam composition when compared to either thermal or low pressure discharge effusive sources. For example, the atomic oxygen translational energies which have been obtained in our laboratory span the range from 0.1–0.5 eV, with future extension of this range up to 0.7 eV being possible for operation with dilute oxygen–helium mixtures. These energies are considerably higher than those accessible with effusive sources constructed from either thoria (ThO_2)[39] or iridium.[40] Also, the atomic oxygen intensity produced by an effusive thermal oven, operating with Knudsen number = 1, would be ca. 4×10^{16} atoms sr^{-1} s^{-1}.[41] This intensity was calculated using an O_2 pressure of 1 Torr, a calculated equilibrium constant of $K_p = 1.2 \times 10^{-2}$ Torr for the process $O_2 \rightleftarrows 2O$ at 2500 K, and assuming that the source orifice was 2 mm high. The fluxes available from low pressure discharge sources are comparable to this, with atomic oxygen fluxes of ca. 3×10^{16} atoms sr^{-1} s^{-1} being realized for operation under effusive flow conditions (with 10% molecular dissociation, a temperature of 350 K,[42] Knudsen number = 1, and a slit height of 2 mm). The above atomic oxygen intensities are much lower than the measured intensities produced by our seeded nozzle source: ca. 5×10^{17} atoms sr^{-1} s^{-1} for oxygen–argon mixtures and $\geq 5 \times 10^{18}$ atoms sr^{-1} s^{-1} for oxygen–helium mixtures. Also note that the Maxwellian velocity distributions typical of effusive sources are quite often too broad for carrying out well defined collision experiments, necessitating the use of mechanical velocity selectors which further reduce their intensity by at least an order of magnitude. It is therefore evident that the nozzle source described here is capable of producing atomic oxygen fluxes which are at least 1–3 orders of magnitude higher than those possible with conventional effusive sources, with the actual intensity gain depending upon the peak velocity and velocity widths which are used for this comparison. The high atomic oxygen fluxes produced by this source should permit extremely well-defined collision experiments to be carried out in which the supersonic beam source would be coupled with either a high resolution mechanical velocity selector or with a magnetic sublevel quantum state selector in order to further define the atomic beam.

The ability of this source to generate seeded beams having high molecular dissociation at pressures up to several hundred Torr total pressure is undoubtedly due to plasma localization at the nozzle tip and to the highly efficient power coupling which has been achieved between the rf tank circuit and the plasma. The use of radio frequency rather than microwave power simplified the above as radio frequency generated plasmas can be easily drawn out of the region enclosed by the coupling coil, while microwave generated plasmas tend to strongly localize in the region surrounded by the coupling cavity. The facile frequency variability and impedance matching of the rf circuitry described earlier also simplifies operation at high pressures. The water cooled nozzle, which ensures extremely stable and reproducible day to day operation of the source, would have to be replaced with a more cumbersome and less efficient oil-cooled design if microwave radiation were used. The ability of this source to generate terminal beams containing $O(^1D_2)$ atoms is at this time unique, and would not have been possible if the discharge were removed from the region immediately behind the orifice.

The atomic oxygen is probably generated in the discharge by a variety of kinetic processes. Thompson[43] has shown, for low pressure discharges, that dissociation can be directly induced by electron-O_2 collisions via the Schumann–Runge continuum $O_2(^3\sum_g^-) \rightarrow [O_2(^3\sum_u^-)] \rightarrow O(^3P_J) + O(^1D_2)$ for collision energies > 7.1 eV. Metastable argon collisions could also lead to dissociation via this process.[11] Metastable helium atoms, due to their high energies, have the ability to Penning ionize molecular oxygen. Ionization in this manner, followed by dissociative recombination between O_2^+ and an electron has been proposed as the primary source of atomic oxygen in oxygen–helium rf discharges.[8]

In addition to oxygen atoms, the plasma is expected to contain metastable rare gas atoms although their concentration and the extent of quenching during nozzle expansion is unknown. Early in the source development, a comparison was made with a conventional electron beam excitation metastable atom source.[45] The flux of metastable argon from the rf discharge source was much less than that from the electron bombardment source. Because the electron beam excitation source is capable of yielding metastable atoms with much narrower velocity distributions, it will probably remain the method of choice for the production of a beam of metastable rare gas atoms. In the study of chemical ionization processes involving oxygen atoms using this beam source, care must be taken to avoid the complication caused by metastable rare gas atoms as well as the UV photons radiated through the nozzle.

The generation of other atomic and electronically excited species should also be possible with this source. In our laboratory we have briefly tested dilute hydrogen–helium mixtures (125 Torr total pressure, 145 W) and have observed atomic hydrogen production. The generation of a supersonic molecular beam containing $O_2(^1\Delta_g)$ without the simultaneous presence of atomic oxygen in the terminal beam should be possible. This

could be accomplished by pulling the discharge back, away from the nozzle tip, and by introducing a small amount of mercury into the gas mixture. The resulting mercuric oxide coating located after the discharge zone would effectively remove the atomic species present in the gas.[44] The feasibility of generating atomic nitrogen beams with a high temperature version of this source is currently being explored in our laboratory.

ACKNOWLEDGMENTS

This work was supported by the Division of Chemical Sciences, Office of Basic Energy Sciences, U.S. Department of Energy under contract No. W-7405-Eng-48 and the Office of Naval Research under contract No. N00014-75-C-0671. We thank Mr. Dane H. Anderberg of the L.B.L. glass shop for his expert assistance during the design and construction of the quartz nozzles, and S.J.S. thanks the Gulf Oil Research Foundation for partial fellowship support.

[a] Present address: Bell Laboratories, 600 Mountain Avenue, Murray Hill, NJ 07974.
[b] Present address: Department of Chemistry, Iowa State University, Ames, IO 50011.

[1] J. T. Herron and R. E. Huie, J. Phys. Chem. Ref. Data **2,** 467 (1973).
[2] S. J. Arnold and H. Rojeska, Appl. Opt. **12,** 169 (1973).
[3] R. J.Madix and A. A. Susu, Surf. Sci. **20,** 377 (1970).
[4] W. D. McGrath and J. J. McGarvey, Planet. Space. Sci. **15,** 427 (1967).
[5] R. J. Cvetanović, Adv. Photochem. **1,** 115 (1963).
[6] J. B. Anderson, R. P. Andres, and J. B. Fenn, in *Advances in Chemical Physics*, edited by J. Ross (Wiley, New York, 1966), Vol. 10, p. 275.
[7] N. Abauf, J. B. Anderson, R. P. Andres, J. B. Fenn, and D. G. H. Marsden, Science **155,** 997 (1967).
[8] D. R. Miller and D. F. Patch, Rev. Sci. Instrum. **40,** 1566 (1969).
[9] P. A. Gorry, C. V. Nowikow, and R. Grice, Chem. Phys. Lett. **49,** 116 (1977).
[10] AD-998 alumina: Coors Porcelain Company, Golden, CO.
[11] H. S. Johnston, *Gas Phase Reaction Kinetics of Neutral Oxygen Species,* Chemical Kinetics Information Center, Nat. Stand. Ref. Data Sys., Nat. Bur. Stand. **20,** (U.S. Government Printing Office, Washington, DC, 1968), p. 4.
[12] H. G. Wagner and J. Wolfrum, Angew. Chem. Int. Ed. Engl. **10,** 604 (1971).
[13] F. K. McTaggart, *Plasma Chemistry in Electrical Discharges* (Elsevier, Amsterdam, 1967), p. 38.
[14] D. DeMaw, Ed., *The Radio Amateur's Handbook,*46th ed. (ARRL, Newington, 1969), p. 44.
[15] D. DeMaw, Ed., *The Radio Amateur's Handbook,* 46th ed. (ARRL, Newington, 1969), p. 49.
[16] K. Henny, Ed., *Radio Engineering Handbook,* 5th ed. (McGraw-Hill, New York, 1959), Chap. 18, p. 23.
[17] Model MN-2000: R. L. Drake Company, Miamisburg, OH.
[18] Paddlewheel flowswitch: Perkin–Elmer Ultek, Inc., Palo Alto, CA.
[19] Carborundum hot pressed boron nitride: Carborundum Co., Refractories and Electronics Division, Latrobe, PA.
[20] Y. T. Lee, J. D. McDonald, P. R. LeBreton, and D. R. Herschbach, Rev. Sci. Instrum. **40,** 1402 (1969).
[21] M. S. Child, *Molecular Collision Theory* (Academic, New York, 1974), p. 3.
[22] W. L. Fite and R. T. Brackman, Phys. Rev. **113,** 815 (1959).
[23] D. Rapp, P. Englander-Golden, and D. D. Broglia, J. Chem. Phys. **42,** 4081 (1965).
[24] J. B. Anderson and J. B. Fenn, Phys. Fluids, **8,** 780 (1965).
[25] J. J. Valentini, Ph.D. dissertation, University of California, Berkeley, CA, 1976.
[26] D. H. Levy, L. Wharton, and R. E. Smalley, in *Chemical and Biochemical Applications of Lasers*, edited by C. B. Moore (Academic, New York, 1977), Vol. 2, p. 1.
[27] D. R. Miller and R. P. Andres, in *Sixth Rarefied Gas Dynamics,* edited by L. Trilling and H. Wachman (Academic, New York, 1969), Vol. 2, p. 1385.
[28] D. R. Miller and R. P. Andres, J. Chem. Phys. **46,** 3418 (1967).
[29] J. G. Skofronik, Rev. Sci. Instrum. **38,** 1628 (1967).
[30] G. Scoles and F. Torello, "Production of Molecular Beams from Free Expanding Jets, Part 1," Report of the Gruppodi Strutture Della Materia del C.N.R., August 1967.
[31] S. Dushman and J. M. Lafferty, Eds., *Scientific Foundations of Vacuum Techniques* (Wiley, New York, 1962), p. 324.
[32] J. B. Anderson, R. P. Andres, and J. B. Fenn, in *Molecular Beams,* edited by J. Ross (Wiley, New York, 1966), p. 312.
[33] D. L. Baulch, D. D. Drysdale, D. G. Horne, and A. C. Lloyd, *Evaluated Kinetic Data for High Temperature Reactions* (Butterworth, London, 1972), Vol. 1a, p. 49.
[34] V. L. Hirschy and J. P. Aldridge, Rev. Sci. Instrum. **42,** 381 (1971).
[35] K. Sköld, Nucl. Instrum. Meth. **63,** 114 (1968).
[36] K. Schofield, J. Photochem. **9,** 55 (1978).
[37] V. Aquilanti, G. Liuti, F. Pirani, F. Vecchiocattivi, and G. G. Volpi, J. Chem. Phys. **65,** 4751 (1976).
[38] J. J. Valentini (private communication).
[39] W. Espe, *Materials of High Vacuum Technology Vol. 12—Silicates* (Pergamon, Oxford, 1968), p. 564.
[40] P. L. Moore, P. N. Clough, and J. Geddes, Chem. Phys. Lett. **17,** 608 (1972).
[41] H. Pauly and J.P. Toennies, in *Methods of Experimental Physics,* edited by B. Bederson and W. L. Fite (Academic, New York, 1968), Vol. 7A, p. 232.
[42] D. St. A. G. Radlein, J. C. Whitehead, and R. Grice, Mol. Phys. **29,** 1813 (1975).
[43] J. B. Thompson, Proc. Roy. Soc. London Ser. A. **262,** 503 (1961).
[44] A. M. Winer and K. D. Bayes, J. Phys. Chem. **70,** 302 (1966).
[45] C. H. Chen, H. Haberland and Y. T. Lee, J. Chem. Phys. **61,** 3095 (1974).